The Astronomical Journal, 148:52 (9pp), 2014 September doi:10.1088/0004-6256/148/3/52

EXCITATION OF THE ORBITAL INCLINATION OF IAPETUS DURING PLANETARY ENCOUNTERS

David Nesvorný[1], David Vokrouhlický[1,2], Rogerio Deienno[1,3], and Kevin J. Walsh[1]
[1] Department of Space Studies, Southwest Research Institute, 1050 Walnut Street, Suite 300, Boulder, CO 80302, USA; davidn@boulder.swri.edu
[2] Institute of Astronomy, Charles University, V Holešovičkách 2, 180 00 Prague 8, Czech Republic
[3] Division of Space Mechanics and Control, National Institute of Space Research, São José dos Campos, SP 12227-010, Brazil
Received 2014 February 24; accepted 2014 June 20; published 2014 August 13

ABSTRACT

Saturn's moon, Iapetus, has an orbit in a transition region where the Laplace surface is bending from the equator to the orbital plane of Saturn. The orbital inclination of Iapetus to the local Laplace plane is $\simeq 8^\circ$, which is unexpected because the inclination should be $\simeq 0$ if Iapetus formed from a circumplanetary disk on the Laplace surface. It thus appears that some process has pumped up Iapetus's inclination while leaving its eccentricity near zero ($e \simeq 0.03$ at present). Here, we examined the possibility that Iapetus's inclination was excited during the early solar system instability when encounters between Saturn and ice giants occurred. We found that the dynamical effects of planetary encounters on Iapetus's orbit sensitively depend on the distance of the few closest encounters. In 4 out of 10 instability cases studied here, the orbital perturbations were too large to be plausible. In one case, Iapetus's orbit was practically unaffected. In the remaining five cases, the perturbations of Iapetus's inclination were adequate to explain its present value. In three of these cases, however, Iapetus's eccentricity was excited to >0.1–0.25, and it is not clear whether it could have been damped to its present value ($\simeq 0.03$) by a subsequent process (e.g., tides and dynamical friction from captured irregular satellites do not seem to be strong enough). Our results therefore imply that only 2 out of 10 instability cases ($\sim$20%) can excite Iapetus's inclination to its current value ($\sim$30% of trials lead to $>5^\circ$) while leaving its orbital eccentricity low.

Key words: planets and satellites: dynamical evolution and stability – planets and satellites: individual (Titan, Iapetus)

Online-only material: color figures

1. INTRODUCTION

The moons of giant planets in the solar system can be divided into several categories. The *regular* moons are large, roughly spherical satellites on nearly circular orbits that are aligned with the host planet's equator. They are thought to have formed by complex accretion processes in the circumplanetary disk (Canup & Ward 2002; Mosqueira & Estrada 2003). The *irregular* moons are smaller, irregularly shaped satellites with large, eccentric, inclined, and often retrograde orbits. They are though to have been captured from heliocentric orbits (e.g., Nesvorný et al. 2007). In addition, there are the ring moons, Neptune's Triton, etc., which are not the main focus here.

Saturn's moon, Iapetus, has a special status among the planetary satellites. Its physical properties, including the large size (diameter $D \simeq 735$ km), nearly spherical figure, and synchronous rotation, are characteristic of a regular moon. Its orbit, however, is unusual in that it is transitional between those of the regular and irregular satellites.

The regular moons, on one hand, have their orbital precession controlled by the quadrupole potential of the host planet's equatorial bulge, and by their mutual interaction. The irregular moons, instead, have their orbital precession driven by solar gravity. The transition between these two regimes occurs near the Laplace radius, $r_{\rm L}$, defined as

$$r_{\rm L}^5 = J_2' R_p^2 a_p^3 \left(1 - e_p^2\right)^{3/2} \frac{M_p}{M_\odot}, \quad (1)$$

where M_p, R_p, a_p, and e_p are the planet's mass, physical radius, semimajor axis, and eccentricity; $M_\odot$ is the solar mass; and

$$J_2' R_p^2 = J_2 R_p^2 + \frac{1}{2} \sum_{i=1}^{n} a_i^2 \frac{m_i}{M_p}. \quad (2)$$

Here J_2 is the quadrupole coefficient, m_i and a_i are the mass and semimajor axis of a satellite, and index i goes over n inner satellites.

For Saturn, $J_2 \simeq 0.0163$, and for Iapetus, $J_2' = 0.065$, mainly contributed by Titan. With the semimajor axis $a = 59\ R_p$, Iapetus is therefore just outside the Laplace radius, $r_{\rm L} \simeq 48\ R_p$. None of other regular or irregular satellites is as close to the Laplace radius. The regular satellites have $a \ll r_{\rm L}$, and their nodal precession is roughly uniform with respect to the planet's equator. The irregular satellites have $a \gg r_{\rm L}$ and their nodal precession is roughly uniform with respect to the orbital plane of their host planet.

In the transition region, $a \sim r_{\rm L}$, the uniform precession occurs with respect to a surface known as the *Laplace surface* that is intermediate between the equatorial and orbital planes. The angle between the planetary spin axis and the normal to the Laplace surface, ϕ, is defined as

$$\tan 2\phi = \frac{\sin 2\theta}{\cos 2\theta + 2r_{\rm L}^5/a^5}, \quad (3)$$

where θ is the host planet obliquity (Tremaine et al. 2009).[4] For Saturn's present obliquity, $\theta_{\rm S} = 26.^\circ 7$, and for the orbital distance of Iapetus, this gives $\phi \simeq 15^\circ$, roughly halfway between the equatorial and orbital planes.

The mean orbital eccentricity of Iapetus is $\simeq 0.03$ and its mean inclination to the Laplace surface is $\simeq 8^\circ$ (Figure 1). If it formed from a circumplanetary disk, one would expect Iapetus to have zero eccentricity and inclination relative to this surface. It thus appears that some process has pumped up Iapetus's inclination while leaving its eccentricity near zero.

[4] Note that Equations (22) and (23) in Tremaine et al. (2009) have typos (corrected, for example, in Tamayo et al. 2013).

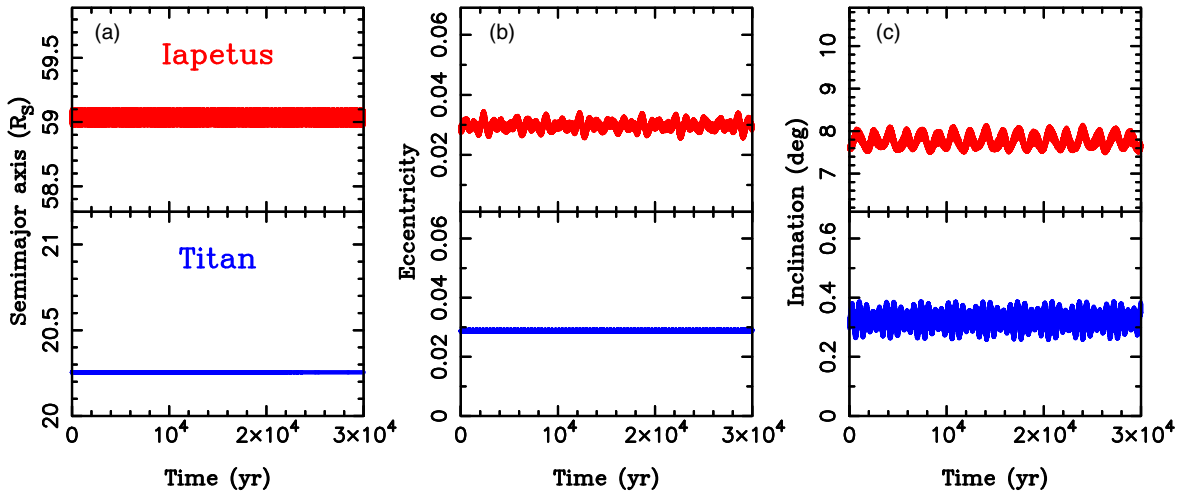

Figure 1. Current orbits of Iapetus (red) and Titan (blue). From left to right, the plots show the semimajor axis, eccentricity, and inclination to the Laplace surface. Notably, the orbital eccentricities of Iapetus and Titan are similar ($\simeq$0.03). The mean orbital inclination of Iapetus to the Laplace surface is $\simeq 8^\circ$ (panel (c)). To make this figure, we obtained the orbital elements of planets and Saturn's satellites from JPL's Horizons (ssd.jpl.nasa.gov). The orbits were numerically integrated from the current epoch to 30,000 yr in the future. We used a fourth-order symplectic map (Nesvorný et al. 2003). The spin axis of Saturn was kept fixed at its current value (ecliptic colatitude $28\overset{\circ}{.}05$, ecliptic longitude $79\overset{\circ}{.}52$; e.g., Ward & Hamilton 2004). The tilt of the Laplace surface was determined from Equation (3), with a small correction for the higher gravitational moments and tilt of Titan's orbit with respect to Saturn's equator.

(A color version of this figure is available in the online journal.)

Ward (1981) pointed out that the shape of the Laplace surface is affected by the mass of the circumplanetary disk, and suggested that the current orbit of Iapetus reflects its shape before the disk dispersed. However, this scenario requires a fast dispersal of the disk in $\sim 10^3$ yr. If the dispersal were slower, the inclination relative to the Laplace surface would behave as an adiabatic invariant and would thus remain near zero.

The excitation of Iapetus's inclination could have instead occurred when Saturn obtained its substantial obliquity. For this to work, the obliquity would need to be tilted on a timescale comparable to Iapetus's nodal precession period (currently $P_\Omega \simeq 3440$ yr). Unfortunately, all processes proposed thus far to explain Saturn's obliquity act too fast (Tremaine 1991) or too slow (Hamilton & Ward 2004; Ward & Hamilton 2004) for this to be plausible.

Here, we study the possibility that Iapetus's inclination was risen to its current value during the (hypothesized) dynamical instability in the outer solar system when scattering encounters of Saturn with ice giants happened (Tsiganis et al. 2005). Our model for dynamical perturbations of the satellite orbits in realistic instability simulations is explained in Section 2. The results are discussed in Section 3. In Section 4, we study the subsequent evolution of Iapetus's orbit to the current epoch. Section 5 concludes this paper.

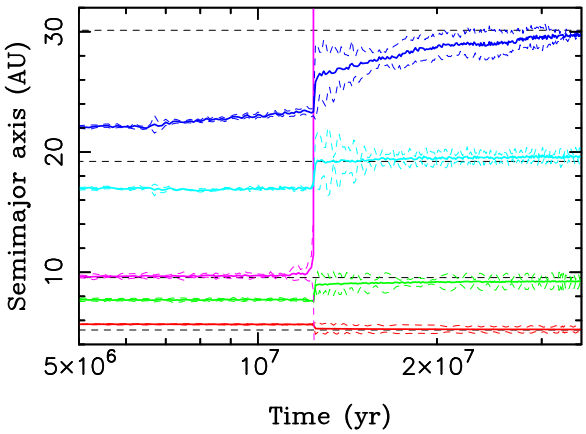

Figure 2. Orbital history of the outer planets in Case 4. Jupiter, Saturn, and the third ice giant with mass $M_{\rm Ice} = 22\ M_\oplus$ were started in the (3:2, 4:3) resonant chain. Uranus and Neptune were placed on non-resonant orbits with semimajor axes 17 AU and 22.1 AU, respectively. The plot shows the semimajor axes (solid lines), and perihelion and aphelion distances (dashed lines) of each planet's orbit. The horizontal black dashed lines show the semimajor axes of planets in the current solar system. The third ice giant was ejected from the solar system at $t = 1.25 \times 10^7$ yr after the start of the integration.

(A color version of this figure is available in the online journal.)

2. MODEL FOR DYNAMICAL PERTURBATIONS OF IAPETUS'S ORBIT DURING PLANETARY ENCOUNTERS

Several properties of the solar system, including the wide radial spacing and orbital eccentricities of the giant planets, can be explained if the early solar system evolved through a dynamical instability followed by migration of planets in the planetesimal disk (Malhotra 1993; Thommes et al. 1999; Tsiganis et al. 2005). Recently, we developed new instability/migration models (Nesvorný & Morbidelli 2012; hereafter NM12), whose initial conditions were tightly linked to our expectations for planet formation in the protoplanetary nebula. We recently used these models to study the orbital behavior of the terrestrial planets during the instability (Brasser et al. 2013), the capture of Jupiter Trojans and irregular satellites (Nesvorný et al. 2013, 2014), and the survival of the Galilean satellites at Jupiter (Deienno et al. 2014).

Here, we work with 10 cases taken from NM12. Cases 1, 2, and 3 were illustrated in Nesvorný et al. (2013, their Figures 1–4). Figure 2 shows the evolution of planets in Case 4. Table 1 lists the main properties of these simulations. Note that these cases were selected solely based on their success in reproducing the orbital properties of the solar system planets (see NM12). We therefore did not have any a priori knowledge of what consequences to expect in these cases for the satellite orbits.

In all cases considered here, the solar system was assumed to have five giant planets initially (Jupiter, Saturn, and three ice

Table 1
The Basic Properties of 10 Selected Instability Cases from NM12

No.	$M_{\rm Ice}$ ($M_\oplus$)	$M_{\rm disk}$ ($M_\oplus$)	No. of Enc.	No. of Enc. in 0.1 AU	$d_{\rm min}$ (AU)
1	15	20	36	0	0.201
2	15	20	51	5	0.021
3	15	20	29	2	0.056
4	22	20	33	2	0.033
5	22	22	22	1	0.007
6	22	22	14	5	0.003
7	18	20	27	1	0.057
8	18	20	17	1	0.020
9	18	20	15	3	0.054
10	18	22	64	6	0.038

Notes. The columns are (1) id number, (2) mass of the third ice giant, (3) mass of the planetesimal disk, (4) number of encounters between Saturn and ice giants, (5) number of encounters with $d < 0.1$ AU, and (6) distance of the closest encounter. Plausible cases that do not lead to excessive perturbations of the orbits of Iapetus and Titan are denoted in bold in Column 1. In Cases 1, 2, and 3, the five planets were placed in a resonant chain (3:2, 3:2, 2:1, 5:3). In Cases 4–10, Jupiter, Saturn, and the third ice giant were placed in a resonant chain (3:2, 4:3), and Uranus and Neptune on non-resonant orbits with semimajor axes 17 AU and 22.1 AU, respectively. The planetesimal disk with mass indicated in Column 3 was represented by 1000 massive disk particles initially located between 24 and 30 AU; see NM12 for additional information on these runs.

giants). This is because NM12 showed that having five planets initially is a convenient way to satisfy constraints. The third ice giant with a mass comparable to that of Uranus or Neptune is ejected into interstellar space during the instability (see also Nesvorný 2011; Batygin et al. 2012). A shared property of the selected runs is that Saturn undergoes a series of encounters with the ejected ice giant.

For each planetary encounter (in all selected cases), we recorded the position and velocity vectors of all planets. Only encounters with $d < R_{\rm H,1} + R_{\rm H,2}$, where d is the distance of planets during the encounter, and $R_{\rm H,1}$ and $R_{\rm H,2}$ are their Hill radii, were considered. The number of these encounters for Saturn is shown in Table 1. In Cases 6 and 10, Saturn had the lowest (14) and highest (64) number of encounters, respectively. To determine the effect of these encounters on Iapetus, we used the recorded states and performed a second set of integrations where Iapetus and Titan were included. This was done as follows.

First, planets were integrated backward in time from the first encounter recorded in the previous integration. This new integration was stopped when $d > 3$ AU. At this point, Titan and Iapetus were inserted in the integration. We assumed that the initial orbits of both satellites were perfectly circular and on the Laplace surface. The semimajor axes were set to their current values ($a_{\rm T} = 20.25\ R_{\rm S}$ and $a_{\rm I} = 59.02\ R_{\rm S}$).[5] Saturn's oblateness and gravity of the inner moons up to Enceladus were included in the forward simulation via the effective quadrupole term J_2' (Equation (2)). The orbits of planets and satellites were propagated forward in time, through the encounter, and up to the point when $d > 3$ AU again. We used the Bulirsch–Stoer integrator with a step of $h = 0.16$ days, which is roughly 1/100 of Titan's orbital period.

Once this part was over, we removed the ice giant that participated in the encounter (to avoid any additional encounters during the interim period), and continued integrating the orbits of planets and satellites toward the next encounter. Ideally, we would like to smoothly join this integration with that corresponding to the next encounter. This is, unfortunately, impossible with our current setup that ignores the gravitational effects of planetesimals (while planetesimals were included in the original simulations). Therefore, even if we integrated the planetary orbits all the way to the next encounter, the position and velocity vectors at that time would not be the same as the ones in the original simulation.

As a compromise, we opted to respect the recorded time interval to the next encounter, δt, if $\delta t < 3500$ yr, or integrate to $t = 3500$–7000 yr if $\delta t > 3500$ yr. The integration time cutoff was implemented to economize the CPU time. This should be correct as long as the timing of encounters is uncorrelated with the orbital phase of the two satellites, which should be a reasonable assumption. The integration was terminated randomly between $t = 3500$ and 7000 yr to ensure that the timing of the next encounter was uncorrelated with the phase of Iapetus's nodal recession.

The orbits of satellites at the end of each integration were used as the initial orbits for the next encounter. To minimize possible discontinuities at this transition, we preserved the osculating values of angles $\Omega_{\rm I}$–$\Omega_{\rm T}$ and $\Omega_{\rm I}$–$\Omega_{\rm S}$, where $\Omega_{\rm T}$ and $\Omega_{\rm I}$ are nodal longitudes of the two satellites with respect to the local Laplace planes, and $\Omega_{\rm S}$ is Saturn's nodal longitude with respect to the invariant plane of the outer solar system. Angle $\Omega_{\rm I}$–$\Omega_{\rm T}$ remained unchanged because we maintained the orientation of the orbits of Titan and Iapetus with respect to Saturn's orbital plane. Angle $\Omega_{\rm I}$–$\Omega_{\rm S}$ was preserved by applying a rotation to the position and velocity vectors of planets before each encounter. This procedure ensured that the secular evolution of $i_{\rm T}$ and $i_{\rm I}$ did not suffer any artificial discontinuities during transitions from one encounter to another. We checked on that, and the discontinuities in $i_{\rm I}$ were found to be $<0.^\circ1$, which should be insignificant.

Saturn's obliquity at the time of planetary encounters is unknown and we therefore treated it as an unknown parameter in our model. In each of the 10 selected cases, we performed two sets of simulations with Saturn's obliquity $\theta_{\rm S} = 0$ and $\theta_{\rm S} = 26.^\circ7$. In the latter case, it is assumed that Saturn's obliquity was excited *before* the instability (Ward & Hamilton 2004; Hamilton & Ward 2004). In the former case, it is assumed that Saturn's equator was aligned with the orbital plane at the onset of the instability. This is plausible, because it has been suggested that Saturn's current obliquity was excited by a secular spin–orbit resonance *after* the instability (Boué et al. 2009). It is also possible that Saturn's obliquity had a value intermediate between these two extremes. We do not study these intermediate values here, because it turns out that satisfactory results can be obtained for both $\theta_{\rm S} = 0$ and $\theta_{\rm S} = 26.^\circ7$ (Section 4). We therefore do not have a good motivation to investigate the intermediate values.

For each case and obliquity value, we performed 1000 integrations where the initial orbital phase of satellites and the initial azimuthal orientation of Saturn's pole were chosen at random. These integrations should be considered statistically equivalent, because the orbital and precessional phases at the onset of instability are unknown. Saturn's spin vector was

[5] The original orbits of Titan and Iapetus before the instability are unknown. Ideally, we would like to start with the initial semimajor axis values that lead, after a period of scattering encounters, to the current ones. This is, unfortunately, difficult to ensure in our forward modeling. This approximation, however, should not be a big deal in the cases where the semimajor axis changes by less than ~10% during scattering encounters, because the results obtained with slightly different initial semimajor axis values are found to be similar.

Table 2
The Orbital Elements of Titan and Iapetus Obtained in Our Scattering Simulations

No.	θ (°)	a_T (R_S)	e_T	i_T (°)	a_I (R_S)	e_I	i_I (°)
		20.25	0.029	0.34	59.02	0.029	8.1
1	0	$20.2535^{+0.0007}_{-0.0007}$	$0.00010^{+0.00007}_{-0.00005}$	$0.17^{+0.11}_{-0.09}$	$59.03^{+0.07}_{-0.09}$	$0.002^{+0.001}_{-0.001}$	$3.2^{+2.0}_{-1.7}$
1	26.7	$20.2535^{+0.0006}_{-0.0006}$	$0.00009^{+0.00005}_{-0.00005}$	$0.33^{+0.17}_{-0.16}$	$59.02^{+0.08}_{-0.07}$	$0.002^{+0.001}_{-0.001}$	$4.0^{+2.6}_{-2.0}$
3	0	$20.2534^{+0.0004}_{-0.0003}$	$0.0012^{+0.0002}_{-0.0002}$	$0.15^{+0.08}_{-0.07}$	$58.3^{+1.8}_{-1.9}$	$0.094^{+0.071}_{-0.044}$	$2.4^{+1.3}_{-1.2}$
3	26.7	$20.2535^{+0.0003}_{-0.0004}$	$0.0006^{+0.0003}_{-0.0002}$	$0.46^{+0.14}_{-0.13}$	$58.4^{+1.7}_{-2.1}$	$0.095^{+0.075}_{-0.045}$	$3.6^{+2.0}_{-1.8}$
4	0	$20.24^{+0.04}_{-0.01}$	$0.005^{+0.001}_{-0.003}$	$0.46^{+0.05}_{-0.04}$	$60.6^{+7.4}_{-6.4}$	$0.151^{+0.069}_{-0.069}$	$6.5^{+2.9}_{-3.3}$
4	26.7	$20.25^{+0.02}_{-0.02}$	$0.0004^{+0.004}_{-0.002}$	$1.5^{+0.4}_{-0.3}$	$60.3^{+7.2}_{-6.5}$	$0.129^{+0.073}_{-0.059}$	$6.9^{+3.8}_{-2.7}$
7	0	$20.2533^{+0.0006}_{-0.0005}$	$0.0005^{+0.0002}_{-0.0002}$	$0.16^{+0.008}_{-0.07}$	$59.01^{+0.25}_{-0.24}$	$0.008^{+0.009}_{-0.004}$	$2.0^{+1.1}_{-0.9}$
7	26.7	$20.2533^{+0.0009}_{-0.0009}$	$0.0004^{+0.0003}_{-0.0002}$	$0.30^{+0.18}_{-0.15}$	$59.04^{+0.23}_{-0.26}$	$0.008^{+0.007}_{-0.005}$	$2.8^{+1.6}_{-1.4}$
8	0	$20.33^{+0.04}_{-0.08}$	$0.030^{+0.012}_{-0.012}$	$0.74^{+0.13}_{-0.12}$	61^{+21}_{-11}	$0.233^{+0.085}_{-0.047}$	$6.6^{+3.4}_{-2.1}$
8	26.7	$20.26^{+0.10}_{-0.08}$	$0.030^{+0.025}_{-0.017}$	$0.91^{+0.59}_{-0.70}$	63^{+20}_{-13}	$0.248^{+0.087}_{-0.066}$	$9.0^{+5.1}_{-5.1}$
9	0	$20.2532^{+0.0005}_{-0.0005}$	$0.0037^{+0.0009}_{-0.0006}$	$1.15^{+0.05}_{-0.06}$	$55.5^{+2.9}_{-2.9}$	$0.24^{+0.14}_{-0.11}$	$5.9^{+3.6}_{-2.1}$
9	26.7	$20.2532^{+0.0004}_{-0.0004}$	$0.004^{+0.002}_{-0.001}$	$1.9^{+0.2}_{-0.8}$	$55.8^{+3.0}_{-2.5}$	$0.24^{+0.12}_{-0.10}$	$8.0^{+4.3}_{-4.1}$

Notes. The columns show (1) id number, (2) Saturn's obliquity (θ_S), (3)–(5) Titan's semimajor axis, eccentricity, and inclination (a_T, e_T, and i_T), and (6)–(8) Iapetus's semimajor axis, eccentricity, and inclination (a_I, e_I, and i_I). The inclinations are given relative to the Laplace surface. The values listed here are the medians and their ±34.1% associated quantiles. The first row with numbers lists the current mean orbital elements of Titan and Iapetus.

assumed to be fixed in inertial space, which should be a reasonable approximation, because the stage of encounters typically last $\sim 10^5$ yr, while the precession period of Saturn's spin axis is much longer ($\simeq 1.8 \times 10^6$ yr at present). Also, note that planetary encounters themselves cannot significantly change the orientation of Saturn's spin axis (Lee et al. 2007).

3. RESULTS OF SCATTERING SIMULATIONS

While the global orbital evolution of the planets was similar in the 10 selected cases, the history of Saturn's encounters with an ice giant varied from case to case. These differences are important for perturbations of Iapetus's orbit and is why different cases were considered in the first place. The statistics of the encounters are reported in Table 1. There are between 14 (Case 6) and 64 (Case 10) recorded encounters in each case, a small fraction of which show a minimal distance $d < 0.1$ AU (Column 5 in Table 1). These very close encounters are obviously the most important for the regular satellites. The closest encounter of all occurred in Case 6 ($d = 0.003$ AU). On the other hand, the closest encounter in Case 1 had $d = 0.201$ AU. For reference, the semimajor axes of Titan and Iapetus are 0.0081 AU and 0.024 AU, respectively.

Cases 2, 6, and 10 had at least five encounters with $d < 0.1$ AU, while Case 5 had one close encounter with $d = 0.007$ AU. These cases generated very large perturbations of orbits of Iapetus and Titan. In most trials, Iapetus was ejected onto a heliocentric orbit. In those in which the orbit remained bound, the eccentricity and inclination ended up implausibly large. In addition, perturbations of Titan's orbit often produced a very large inclination that, again, cannot be reconciled with the current orbit (because there is no obvious means to damp Titan's inclination back down; see Section 3). We therefore believe that these cases are implausible.

This is interesting, because it shows that Saturn's regular satellites pose important constraints on the instability calculations. Deienno et al. (2014) used Cases 1–3 from NM12 discussed here and considered constraints from the Galilean satellites of Jupiter. They found Case 2 implausible, because perturbations of the orbits of the Galilean satellites were clearly excessive. This finding correlates with the constraints from the Saturnian satellites considered here, which also allow us to rule out Case 2.

Table 2 shows the orbital elements of Titan and Iapetus after the last planetary encounter in Cases 1, 3, 4, 7, 8, and 9. The range of the results is broad, starting from relatively small perturbations such as those in Case 7, where Iapetus inclinations ended up being $2° < i_I < 3°$ on average. Only $\simeq$10% of trials in this case exceeded 5°. We therefore find that dynamical perturbations in Case 7 are not large enough to explain Iapetus's current inclination. This implies that Iapetus would need to have a significant inclination before the stage of encounters.

Cases 1, 3, 4, 8, and 9 appear to be more interesting. We now discuss these cases in detail. In general, the results show a dependence on the obliquity value of Saturn. In Case 1, for example, Iapetus's orbit reached inclination $i_I = 3.^\circ 2^{+2.0}_{-1.7}$ for $\theta_S = 0$, while $i_I = 4.^\circ 0^{+2.6}_{-2.0}$ for $\theta_S = 26.^\circ 7$. This trend of increasing i_I with increasing θ_S is expected because of the following arguments. With $\theta_S = 0$, the main source of the inclination excitation is the direct torque of the ice giant on the satellite orbit. If θ_S is non-zero, however, the inclination with respect to the Laplace surface can be changed by several additional effects.

These additional effects are *indirect* in that they do not change the orientation of the satellite orbital plane in the inertial reference frame. Instead, they affect the tilt of the Laplace surface. A change in the semimajor axis of a satellite, for example, implies a change of ϕ according to Equation (3). If the semimajor axis immediately changed back during the next planetary encounter, the original orbital inclination would be recovered. If, instead, the next encounter happens only after a significant fraction of the nodal period, the satellite's orbital plane has time to recess around the Laplace surface, and the original inclination is not recovered.

Both of these cases occur in reality, as there are typically a few dozen encounters spread over $\sim 10^5$ yr (while $P_\Omega = 3440$ yr). Therefore, as the semimajor axis changes as a result of

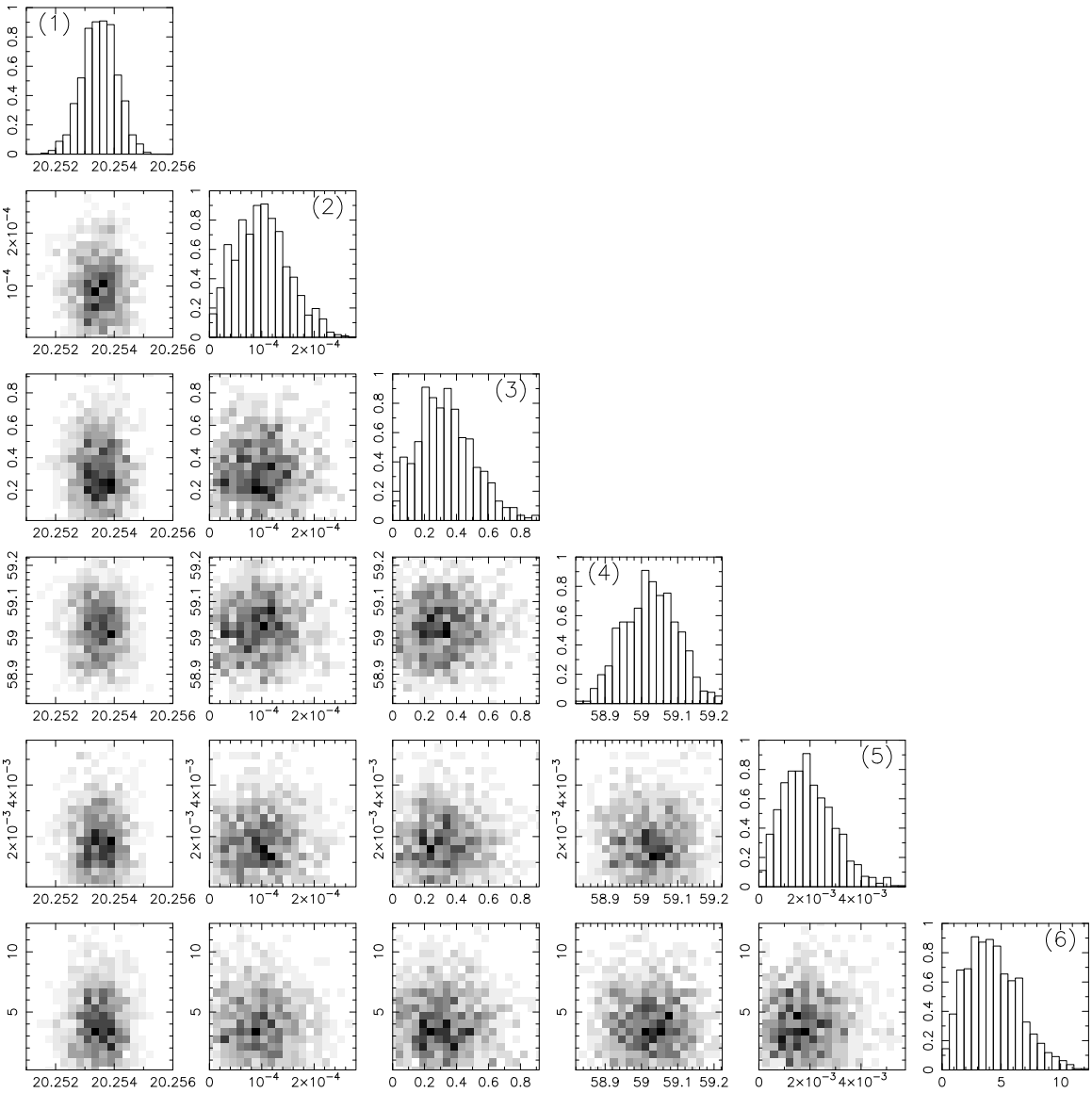

Figure 3. Final distribution of orbital elements obtained in Case 1 and $\theta_S = 26.^\circ7$. The plots show the one-dimensional (1D) histograms and two-dimensional (2D) projections of the (1) semimajor axis of Titan (the units are R_S), (2) eccentricity of Titan, (3) inclination of Titan (in degrees), (4) semimajor axis of Iapetus (in R_S), (5) eccentricity of Iapetus, and (6) inclination of Iapetus (in degrees). Darker bins in the 2D projections correspond to a larger likelihood of the result. The inclinations are given with respect to the Laplace surface.

encounters, the inclination will randomly walk with respect to the Laplace surface. This effect adds to that produced on the satellite orbit by the direct torque. Additional changes in a satellite's orbital inclination relative to the Laplace surface are produced, as *Saturn's* orbit is modified by scattering encounters with ice giants. They are a consequence of changes in Saturn's orbital inclination and the dependence of ϕ on Saturn's semimajor axis in Equation (1). For example, $\phi \simeq 20^\circ$ at 59 R_S for Saturn's initial semimajor axis $a_S \simeq 7.8$ AU (Figure 2), while $\phi \simeq 15^\circ$ with the present value $a_S \simeq 9.55$ AU.

Figure 3 shows the final distribution of orbital elements of Iapetus and Titan obtained in Case 1 and $\theta_S = 26.^\circ7$. This result is encouraging for several different reasons. First, the final $i_I > 5^\circ$ in about 30% of all trials. The probability that Iapetus obtained its present orbital inclination ($\simeq 8^\circ$) is therefore significant. Second, Titan's inclination to the Laplace surface was excited to values between $0.^\circ1$ and $0.^\circ6$, with the distribution peaking at $\simeq 0.^\circ4$. This is consistent with the present inclination of Titan ($\simeq 0.^\circ34$ mean). Third, the orbital eccentricity of Iapetus remained low. There is thus no need in this case to invoke tides or other effects to bring the eccentricity down.

Figure 4 shows the orbital elements of satellites at the end of each encounter in one trial integration in Case 1. This trial was selected and is shown here because it leads to the final values of the orbital elements that are fully consistent with the present orbits of Titan and Iapetus. The semimajor axis values remained nearly unchanged, eccentricities remained small,[6] and inclinations reached the required values. Many trial integrations in Case 1 show a similar result.

The results in Case 1 and $\theta_S = 0$ are less ideal, because only $\simeq$15% of trials lead to $i_I > 5^\circ$. This is a consequence of the general dependence of the results on Saturn's obliquity discussed above. We conclude that a significant initial obliquity of Saturn before the stage of planetary encounters helps to obtain

[6] This would imply that the present orbital eccentricities of $\simeq$0.03 of Titan and Iapetus were produced by a different process that can pre-date the time of the planetary instability.

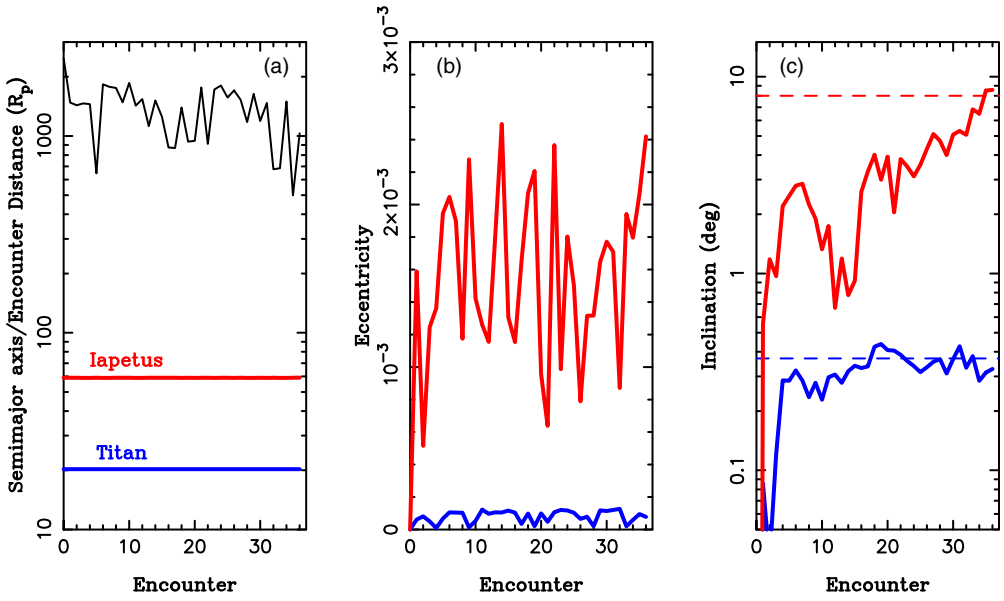

Figure 4. Example of the satellite orbit evolution in Case 1. From left to right, the panels show the semimajor axis, eccentricity, and inclination of Iapetus (red) and Titan (blue). The black line in panel (a) shows the minimal distance of Saturn and the ice giant for each encounter. The dashed lines in panel (c) indicate the current inclination values of the orbits. Here, we assumed that $\theta_S = 26.^\circ7$. The inclinations are given with respect to the Laplace surface.

(A color version of this figure is available in the online journal.)

better results in Case 1. Very similar results were obtained in Case 3. We therefore do not explicitly discuss Case 3 here.

Case 4 tells a different story. In this case, the closest encounter occurred at a distance $d = 0.033$ AU, which is only $\simeq$1.3 times the semimajor axis of Iapetus. This encounter itself generated a larger perturbation of satellite orbits than all encounters in Cases 1 and 3. Iapetus's inclination ended up being $6.^\circ5^{+2.9}_{-3.3}$ for $\theta_S = 0$ (Figure 5) and $6.^\circ9^{+3.8}_{-2.7}$ for $\theta_S = 26.^\circ7$. Both of these results match the current inclination of Iapetus comfortably within 1σ.

Interestingly, Titan's inclination was excited to $0.^\circ458^{+0.048}_{-0.041}$ for $\theta_S = 0$ and to $1.^\circ53^{+0.43}_{-0.25}$ for $\theta_S = 26.^\circ7$. Thus, based solely on this result, Saturn's low obliquity would be preferred in Case 4, because Titan's inclination ends up matching its current value better with $\theta_S = 0$ than when the obliquity is large. This is opposite to what we have found for Cases 1 and 3 (see above).

In addition, unlike in Cases 1 and 3, the eccentricity of Iapetus became significantly excited in Case 4 (to $0.151^{+0.069}_{-0.069}$ for $\theta_S = 0$ and to $0.129^{+0.073}_{-0.059}$ for $\theta_S = 26.^\circ7$). This case would thus require significant eccentricity damping in times after the planetary instability (Section 4). Figure 6 illustrates the orbital elements of Iapetus and Titan in one trial integration in Case 4.

Cases 8 and 9 bear similarities to Case 4 (Table 2). Both of these cases generated the required excitation of Iapetus's inclination, but led to significant eccentricity that would need to be damped after the epoch of planetary encounters. Titan's inclination obtained in these simulations was roughly correct, perhaps only a bit larger than what we would ideally like (Column 5 in Table 2). Titan's eccentricity remained essentially unchanged.

These results should be seen in positive light. We were only able to consider 10 instability cases thus far. Our resolution of the initial conditions leading to the instability and planetary encounters is therefore grainy. Given the sensitivity of these results to the detailed history of planetary encounters, we then find it quite possible that our tests are somewhat inadequate. A more thorough investigation of parameter space will require massive CPU use or a different approach (D. Vokrouhlický et al., in preparation).

4. SUBSEQUENT ORBITAL EVOLUTION OF IAPETUS FROM AFTER THE INSTABILITY TO THE CURRENT EPOCH

It is hypothesized that planetary instability occurred $\simeq$4 Gyr ago (e.g., Gomes et al. 2005). Here, we studied several dynamical processes that may have altered Iapetus's orbit during the gigayears after the instability. We looked into several mechanisms: (1) dynamical effects of flybys of 100 km class planetesimals, (2) dynamical friction from captured irregular satellites and their debris, and (3) tides. Our tests showed that the effects of (1) are completely negligible. Mechanism (2) would be effective in damping Iapetus's eccentricity only if the mass captured in (or evolved to) the neighborhood of Iapetus's orbit were $>0.1\,M_{\rm Iapetus}$, where $M_{\rm Iapetus} = 1.8\times10^{21}$ kg. For comparison, the mass of the original population of irregular satellites captured at Saturn is estimated to be $\sim10^{18}$ kg (Nesvorný et al. 2014), more than two orders of magnitude lower than required.

To study (3), we adopted a model for tides developed in Mignard (1979, 1980), where the tidal accelerations of satellites are given as functions of the planetocentric Cartesian coordinates (Equations (1) and (2) in Lainey et al. 2012). The tidal evolution of a satellite's orbit was studied using direct numerical integrations of orbits with a symplectic N-body code known as `swift_rmvs3` (Levison & Duncan 1994) that we modified to include Mignard's tidal acceleration terms. The satellite rotation was assumed to be synchronous.[7]

[7] To implement the synchronous rotation in the code, we adopted the following approximation (V. Lainey 2014, private communication). For tides raised on a satellite, we only included the radial component of the acceleration. This component does not depend on a satellite's rotation rate, and is therefore independent of the detailed assumptions about synchronicity. We then multiplied the magnitude of this component by 7/3 to account for the effects of the longitudinal component of the tidal acceleration. This is because in the limit of small eccentricities, which is applicable here, the orbital energy dissipated by radial flexing of the satellite is 3/4 of that dissipated by satellite's librations (e.g., Murray & Dermott 1999, chapter 4).

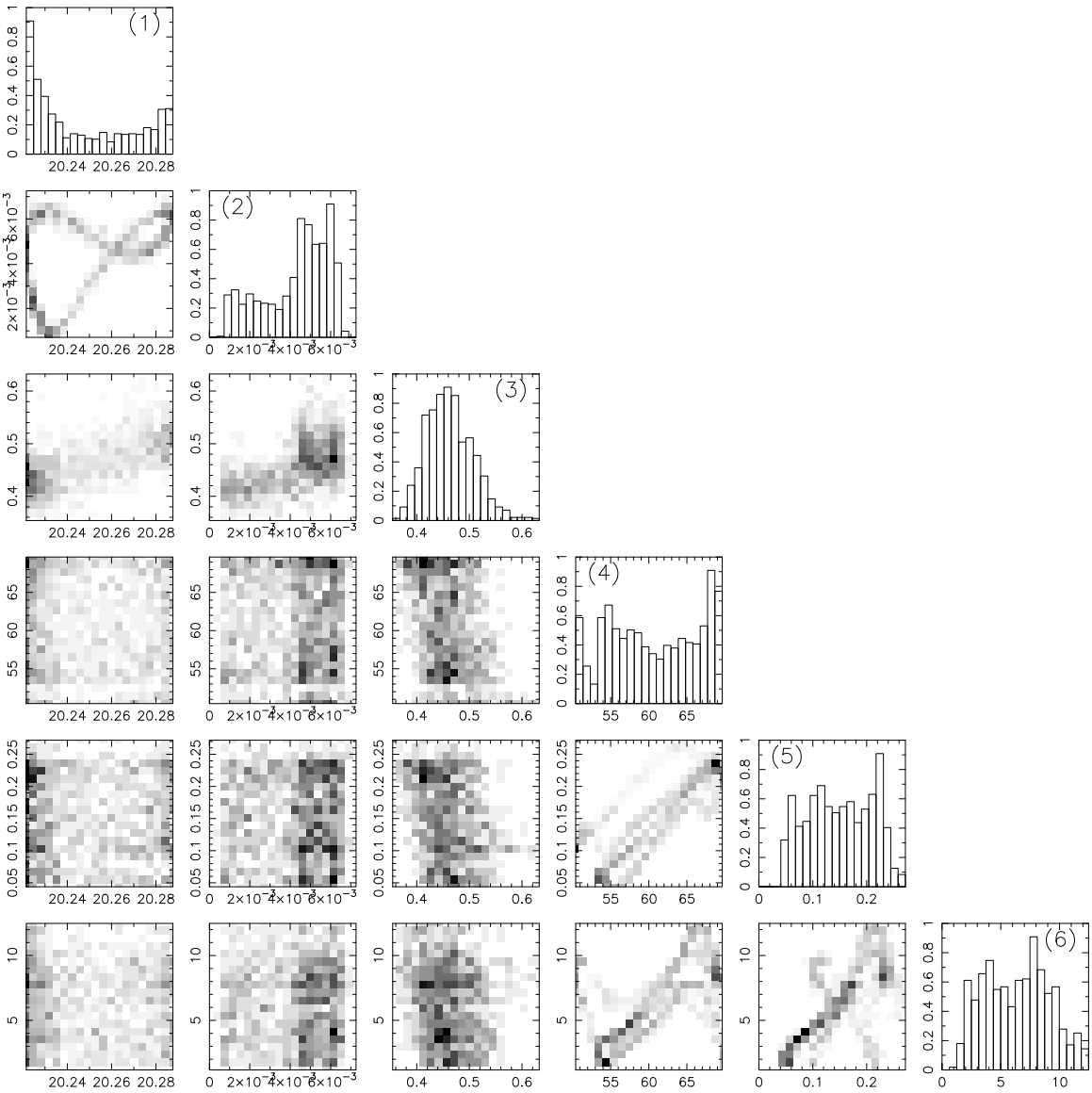

Figure 5. Final distribution of orbital elements obtained in Case 4 and $\theta_S = 0$. The plots show the 1D and 2D projections of the (1) semimajor axis of Titan (the units are R_S), (2) eccentricity of Titan, (3) inclination of Titan (in degrees), (4) semimajor axis of Iapetus (in R_S), (5) eccentricity of Iapetus, and (6) inclination of Iapetus (in degrees). Darker bins in the 2D projections correspond to a larger likelihood of the result. The inclinations are given with respect to the Laplace surface.

The dissipation effects were parameterized by the standard tidal parameter $Q' = Q/k_2$, where k_2 is the quadrupole Love number and Q is the quality factor (assumed constant here). As for Saturn, previous theoretical work indicated the Q' values at least of the order of 10^4 (e.g., Peale et al. 1980; Zhang & Nimmo 2009), but Lainey et al. (2012) recently suggested from the astrometric modeling of *Cassini*'s observations that $Q' \simeq 4350$ (with about 30% uncertainty). We use this later value, but point out that our main conclusions (related to the eccentricity of Iapetus) are essentially independent of Saturn's Q'.

Instead, the strength of tidal damping of the eccentricity of Iapetus sensitively depends, via the secular orbital coupling of Iapetus to other moons,[8] on the dissipation of tidal energy in Titan and the inner satellites. We find that it is problematic to quantify this process, because Q' values of Saturn's satellites are poorly known. We therefore performed several numerical integrations with widely ranging values of Q'. All satellites between Mimas and Iapetus were included.

The principal result of these integrations is that the secular coupling of Iapetus to Titan and the inner moons, and the tidal dissipation in Titan and the inner moons, would potentially be capable of reducing Iapetus's eccentricity only if $Q' \lesssim 20$ (Figure 7). This low value of Q', however, appears to be implausible. For example, dynamical constraints suggest that $Q' \simeq 10^3$–10^4 for Enceladus and Dione (Zhang & Nimmo 2009). For Titan, theory indicates that the strength of tidal dissipation should sensitively depend on its interior structure (e.g., Sohl et al. 1995), but is unlikely to be as low as needed here. Measurements elsewhere in the solar system suggest $Q' \simeq 70$ for Io (Lainey et al. 2009) and $Q' \simeq 1200$ for the Moon (Khan et al. 2004).

In summary, we find that if the orbital eccentricity of Iapetus had become excited during planetary encounters, it would probably have stayed high to the current epoch. This result has important implications for the interpretation of our scattering

[8] Iapetus itself is too far from Saturn for direct tides to be important for Iapetus's orbital evolution.

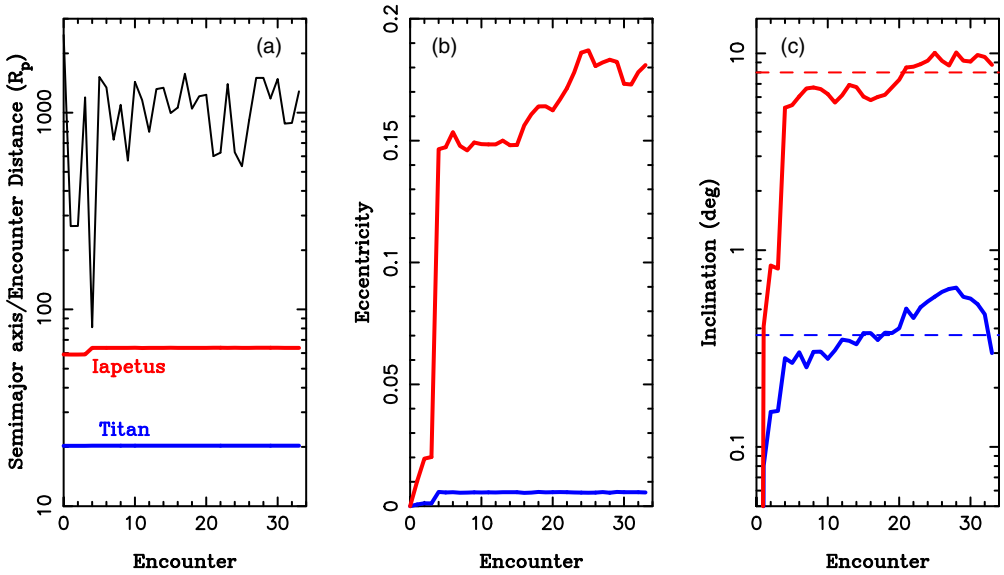

Figure 6. Example of the satellite orbit evolution in Case 4. From left to right, the panels show the semimajor axis, eccentricity, and inclination of Iapetus (red) and Titan (blue). The black line in panel (a) shows the minimal distance of Saturn and the ice giant for each encounter. The dashed lines in panel (c) indicate the current inclination values of the orbits. Here, we assumed that $\theta_S = 0$. The inclinations are given with respect to the Laplace surface.

(A color version of this figure is available in the online journal.)

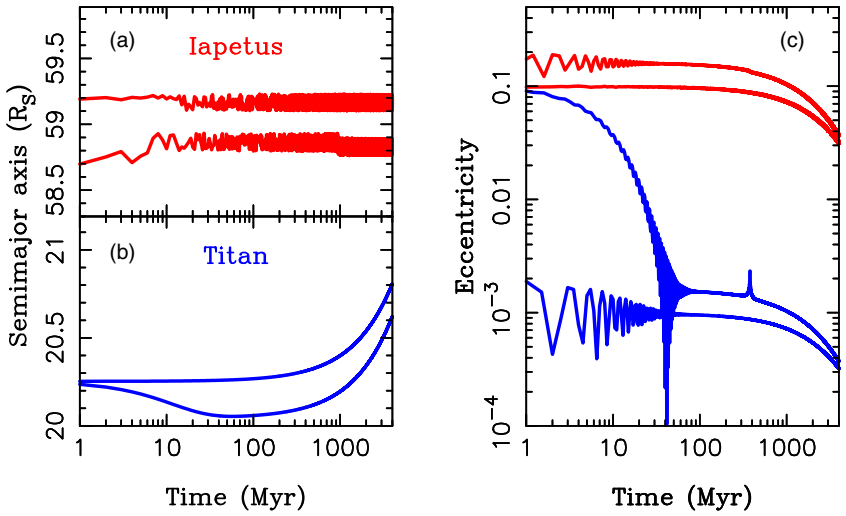

Figure 7. Examples of the orbital evolution of Titan (blue) and Iapetus (red) due to tides. Two cases with different initial setups are shown here: (1) $e_T = 0$ and $e_I = 0.1$, and (2) $e_T = 0.1$ and $e_I = 0.2$. In panel (a), the two tracks of Iapetus were offset by ± 0.2 R_S for clarity. The orbital inclinations of Titan and Iapetus, not shown here, do not practically change over 4 Gyr. The final eccentricity of Iapetus, after 4 Gyr of tidal evolution, is roughly equal to the current value ($e_I \simeq 0.029$). In both cases, we fixed $Q'_S = 4350$ (Lainey et al. 2012) and used the same value of Q' for all satellites, $Q' = 20$, and $Q' = 10$, respectively, for the two initial setups. The extremely strong tidal dissipation in satellites implied by these values is probably implausible (see the text). Note that Titan and Iapetus were started with their current semimajor axis value in these simulations, which is, strictly speaking, incorrect; see Ćuk et al. (2013) for a more detailed analysis of the orbital history of Titan and Iapetus.

(A color version of this figure is available in the online journal.)

experiments (Section 3), because it shows that only 3 out of 10 instability cases considered here (numbers 1, 3, and 7 in Table 2) appear to be plausible based on Iapetus's eccentricity constraint. We also find that Titan's and Iapetus's orbital inclinations, if excited by planetary encounters, would remain essentially unchanged during the subsequent tidal evolution. Titan's inclination (current mean $i_T = 0.^\circ34$) does not appear to be a problem because it stays low during the scattering phase in all three cases mentioned above. While Case 7 would require that Iapetus's inclination was excited already before the scattering phase, Cases 1 and 3 are capable of generating Iapetus's inclination during the scattering phase (Figure 4).

5. CONCLUSIONS

The orbital inclination of Iapetus is a long-standing problem in planetary science. The inclination should be $\simeq 0$ if Iapetus formed from a circumplanetary disk on the Laplace surface, but it currently is $\simeq 8^\circ$. Here, we investigated the possibility that Iapetus attained its significant orbital inclination during a hypothesized instability in the outer solar system when Saturn had close encounters with an ice giant. We found that roughly 50% of instability cases that satisfy other constraints (see NM12) are capable of exciting Iapetus's (and Titans's) inclination to the current value. For most of these cases to be plausible, however, some dissipation mechanism is required to damp the orbital

eccentricity of Iapetus that is typically excited by encounters to >0.1. In only 2 out of 10 instability cases studied here, the eccentricity of Iapetus remained low while the orbital inclination of Iapetus was significantly excited (such that $i_1 > 5°$ in at least 30% of trials; Cases 1 and 3). These different outcomes depend on the number and minimum distance of the encounters, and on their geometry.

One of our main motivations for this study was the question of whether it is possible to have a history of encounters between Saturn and an ice giant that leads to capture of the irregular satellites at Saturn via the mechanism described in Nesvorný et al. (2007) and to satisfy constraints from Saturn's regular satellites. Here, we demonstrated that it is indeed possible to satisfy these constraints simultaneously (e.g., in Cases 1 and 3; see Nesvorný et al. 2014 for irregular satellite capture in these cases). Moreover, we found that the orbital perturbation of the regular satellites mainly results from a few of the closest encounters. The results are therefore expected to be highly variable. As a rough criterion, we find that the closest encounter of the ice giant to Saturn cannot be closer than 0.05 AU, or about two times the semimajor axis of Iapetus (or 0.02 AU if the eccentricity constraint is relaxed). Capture of irregular satellites, on the other hand, mainly depends on the bulk of distant encounters, and is expected to occur generically. The regular and irregular satellites thus represent somewhat different, and not mutually exclusive, constraints.

Our final remark is related to the orbital perturbations of regular satellites at Jupiter, Uranus, and Neptune. Deienno et al. (2014) already demonstrated that the orbits of the Galilean satellites remain unchanged in Case 3 studied here, while they suffer implausibly large excitations in Case 2. Also, according to Deienno et al., from the perspective of the Galilean moons, Case 1 is intermediate between Cases 2 and 3. Our tests for Jupiter, using the same methodology as described for Saturn in Section 2, confirm these results and show, in addition, that Cases 4, 7, 8, and 10 generate only modest (and plausible) perturbations of the Galilean satellite orbits. Therefore, while there is a hint of correlation of the results for Jupiter and Saturn, there are also cases such as Case 10, where the Galilean moons survive essentially undisturbed while Saturn's regular satellites, including Titan, plunge into disorder. These cases could give the right framework for the hypothesis of the late origin of the Saturn system (Asphaug & Reufer 2013).

Interestingly, the satellites of Uranus are a very sensitive probe for planetary encounters. This is because the most distant of these satellites, Oberon, has a semimajor axis comparable to Rhea in the Saturnian system, and only $\simeq 0\overset{\circ}{.}068$ inclination with respect to the Laplace surface. Previous works performed in the framework of the original Nice model and the jumping-Jupiter model with four planets (Deienno et al. 2011; Nogueira et al. 2013; R. Gomes 2014, private communication) had difficulties satisfying this constraint, because Uranus experienced many encounters with Jupiter and/or Saturn in these instability models. In the models taken from NM12, however, Uranus does not have encounters with Jupiter and Saturn, and instead experiences a relatively small number of encounters with a relatively low-mass ice giant. According to our tests, Oberon's inclination remains below $0\overset{\circ}{.}1$ in all cases studied here, except for Case 8. This result could be used to favor the NM12 instability models. Neptune's satellites are less of a constraint in this context, because Triton's orbit is closely bound to Neptune and has been strongly affected by tides (Correia 2009).

This work was supported by NASA's Outer Planet Research program. The work of D.V. was partly supported by the Czech Grant Agency (grant P209-13-013085). R.D. was supported by FAPESP (grants 2010/11109 and 2012/23732). We thank Matija Ćuk for a very helpful referee report.

REFERENCES

Asphaug, E., & Reufer, A. 2013, Icar, 223, 544
Batygin, K., Brown, M. E., & Betts, H. 2012, ApJL, 744, L3
Boué, G., Laskar, J., & Kuchynka, P. 2009, ApJL, 702, L19
Brasser, R., Walsh, K. J., & Nesvorný, D. 2013, MNRAS, 433, 3417
Canup, R. M., & Ward, W. R. 2002, AJ, 124, 3404
Correia, A. C. M. 2009, ApJL, 704, L1
Ćuk, M., Dones, L., & Nesvorný, D. 2013, arXiv:1311.6780
Deienno, R., Nesvorný, D., Vokrouhlický, D., & Yokoyama, T. 2014, AJ, submitted
Deienno, R., Yokoyama, T., Nogueira, E. C., Callegari, N., & Santos, M. T. 2011, A&A, 536, A57
Gomes, R., Levison, H. F., Tsiganis, K., & Morbidelli, A. 2005, Natur, 435, 466
Hamilton, D. P., & Ward, W. R. 2004, AJ, 128, 2510
Khan, A., Mosegaard, K., Williams, J. G., & Lognonné, P. 2004, JGRE, 109, 9007
Lainey, V., Arlot, J.-E., Karatekin, Ö., & van Hoolst, T. 2009, Natur, 459, 957
Lainey, V., Karatekin, Ö., Desmars, J., et al. 2012, ApJ, 752, 14
Lee, M. H., Peale, S. J., Pfahl, E., & Ward, W. R. 2007, Icar, 190, 103
Levison, H. F., & Duncan, M. J. 1994, Icar, 108, 18
Malhotra, R. 1993, Natur, 365, 819
Mignard, F. 1979, M&P, 20, 301
Mignard, F. 1980, M&P, 23, 185
Mosqueira, I., & Estrada, P. R. 2003, Icar, 163, 198
Murray, C. D., & Dermott, S. F. 1999, Solar System Dynamics (Cambridge: Cambridge Univ. Press)
Nesvorný, D. 2011, ApJL, 742, L22
Nesvorný, D., Alvarellos, J. L. A., Dones, L., & Levison, H. F. 2003, AJ, 126, 398
Nesvorný, D., & Morbidelli, A. 2012, AJ, 144, 117 (NM12)
Nesvorný, D., Vokrouhlický, D., & Deienno, R. 2014, ApJ, 784, 22
Nesvorný, D., Vokrouhlický, D., & Morbidelli, A. 2007, AJ, 133, 1962 (NVM07)
Nesvorný, D., Vokrouhlický, D., & Morbidelli, A. 2013, ApJ, 768, 45
Nogueira, E. C., Gomes, R. S., & Brasser, R. 2013, AAS/Division of Dynamical Astronomy Meeting, 44, 204.21
Peale, S. J., Cassen, P., & Reynolds, R. T. 1980, Icar, 43, 65
Sohl, F., Sears, W. D., & Lorenz, R. D. 1995, Icar, 115, 278
Tamayo, D., Burns, J. A., Hamilton, D. P., & Nicholson, P. D. 2013, AJ, 145, 54
Thommes, E. W., Duncan, M. J., & Levison, H. F. 1999, Natur, 402, 635
Tremaine, S. 1991, Icar, 89, 85
Tremaine, S., Touma, J., & Namouni, F. 2009, AJ, 137, 3706
Tsiganis, K., Gomes, R., Morbidelli, A., & Levison, H. F. 2005, Natur, 435, 459
Ward, W. R. 1981, Icar, 46, 97
Ward, W. R., & Hamilton, D. P. 2004, AJ, 128, 2501
Zhang, K., & Nimmo, F. 2009, Icar, 204, 597